



ALMA MATER STUDIORUM
UNIVERSITÀ DI BOLOGNA

ARCHIVIO ISTITUZIONALE
DELLA RICERCA

Alma Mater Studiorum Università di Bologna Archivio istituzionale della ricerca

Accidental release in the bunkering of LNG: Phenomenological aspects and safety zone

This is the final peer-reviewed author's accepted manuscript (postprint) of the following publication:

Published Version:

Accidental release in the bunkering of LNG: Phenomenological aspects and safety zone / Carboni M.; Pio G.; Mocellin P.; Vianello C.; Maschio G.; Salzano E.. - In: OCEAN ENGINEERING. - ISSN 0029-8018. - ELETTRONICO. - 252:(2022), pp. 111163.1-111163.9. [10.1016/j.oceaneng.2022.111163]

Availability:

This version is available at: <https://hdl.handle.net/11585/897320> since: 2022-10-25

Published:

DOI: <http://doi.org/10.1016/j.oceaneng.2022.111163>

Terms of use:

Some rights reserved. The terms and conditions for the reuse of this version of the manuscript are specified in the publishing policy. For all terms of use and more information see the publisher's website.

This item was downloaded from IRIS Università di Bologna (<https://cris.unibo.it/>).
When citing, please refer to the published version.

(Article begins on next page)

Accidental Release in the Bunkering of LNG: Phenomenological Aspects and Safety Zone

*Mattia CARBONI¹, Gianmaria PIO², Paolo MOCELLIN¹, Chiara VIANELLO¹,
Giuseppe MASCHIO¹, Ernesto SALZANO^{2,*}*

¹ Dipartimento di Ingegneria Industriale, Università degli Studi di Padova. Via
Marzolo 9, 35131 Padova, Italia

² Dipartimento di Ingegneria Civile, Chimica, Ambientale e dei Materiali,
Università degli studi di Bologna, Via Terracini 28, 40131 Bologna, Italia

*Author to whom correspondence should be addressed: ernesto.salzano@unibo.it

Abstract

The continuous increase in consciousness on properties and models characterizing cryogenic fuels has opened a new era for the supply of alternative sources of energy, especially in the naval sector. However, practical insights providing comprehensive indications for the development of safe and optimized procedures are still missing or lacking. In this perspective, a preliminary investigation on the commonly adopted procedure was integrated with a 3-dimensional representation of a typical port area in computational fluid dynamics (CFD) simulations implementing sub-models suitable for cryogenic conditions. At first, different scenarios were selected as representative for possible release conditions: Unloading Operation (UO), Shore to Ship (STS), and Truck to Ship (TTS) bunkering operations. This study indicates that TTS can be the most critical scenario because of the simultaneity of bunkering and disembarking procedures. The numerical analysis was devoted to the quantification of the safety distance in the case of the absence of an ignition source. The area where skin and eyes' frostbite are possible is assessed, as well, based on the combination of estimated temperature and local wind speed. The resulting safety distances were compared against estimations deriving by discrete and integral models without obstacles, demonstrating that neglect obstacles lead to non-conservative results. Indeed, a local increase in mixing effectiveness, limiting the flammable area within the channel between quayside and ship, was identified and characterized in this work. Besides, it was found that only under certain circumstances for TTS operations a flammable cloud can potentially reach passengers. Hence, the installation of barriers and mitigation systems (e.g., water curtains) is strongly recommended.

Keywords: Liquefied Natural Gas; Dispersion; Bunkering; Safety; Numerical Modelling.

Highlights:

- Evaluation of safety distances on downwind direction after an LNG release
- Integration of CFD analysis with simplified 3D ports
- Comparison of estimations deriving by integral and discrete models
- Assessment of flammable region, height, and volume
- Quantification of the area where frostbite is possible

41

1. Introduction

42 The use of liquefied natural gas (LNG) has been significantly promoted by economic, environmental,
43 political, and logistic factors (Chen et al., 2017)(Osorio-Tejada et al., 2017), raising new concerns on
44 safety aspects due to the cryogenic conditions and interactions with industrial operators working in the
45 port areas (Fy et al., 2016)(Chang and Park, 2019)(Aneziris et al., 2020). As a way of example, frostbite
46 is the freezing of skin and tissues due to the instantaneous contact with cold substances or surfaces and
47 can be categorized as first degree (superficial, "frostnip"), second degree (full skin), third-degree
48 (subcutaneous tissue), and fourth-degree (extensive tissue and bone). It occurs when the temperature of
49 the skin or the tissues is lower than 2 °C (for the short duration exposure), thus resulting in the formation
50 of intracellular ice crystals and microvascular occlusion (Weinzweig, 2010). Similarly, freeze burns
51 refer to damages produced by the prolonged exposure time of the human body to cold atmosphere or
52 surfaces. Few cases are reported in the literature for LNG frostbites, whereas other reports can be found
53 for other cryogenic liquids (Kumar and Chirayil, 1999) (Uygur et al., 2009) (Sever et al., 2008).

54 In this sense, the realization of a quantitative risk assessment (QRA) is highly desirable. This analysis
55 can be intended as a combination of probabilistic and phenomenological approaches. The former aims
56 at the assessment of the probability of a given scenario, whereas the latter quantifies the consequences
57 related to this event. In both cases, results can be affected by several parameters. As a way of example,
58 an accidental release of LNG can result in a pool fire, flash fire, or atmospheric dispersion based on the
59 presence of immediate or delayed ignition, as reported in the literature (Pio and Salzano, 2019). The
60 selection of specific scenarios should be driven by the probabilistic approach (Paik, 2020). However, it
61 usually considers local parameters (e.g., atmospheric conditions) and peculiarity of the analyzed plant,
62 showing a case-specific nature. On the other hand, some generalizations can be done to identify critical
63 aspects in the commonly adopted procedures. In this view, ISO 20519: 2017 (ISO 20519, 2017) and
64 ISO/TS 18683: 2015 (Publication, 2015) standards indicate bunkering as the most critical operation,
65 suggesting procedures for the definition of safety zones and allowed activities. Once the scenario is
66 identified, several procedures can be used for the quantification of safety distances associated to floating
67 facilities during bunkering operations (Park et al., 2020). Besides, safety distances can be significantly
68 affected by wind speed, wind direction, ship geometry and loading conditions (Park et al., 2018),
69 suggesting the realization of dedicated investigations aiming at their quantification.

70 Different modalities can be adopted for the loading procedures in the naval sector such as: 1) LNG
71 Unloading Operation (UO); 2) LNG Shore to Ship (STS) or Port to Ship (PTS); 3) Truck to Ship (TTS);
72 4) Ship to Ship (StS). In the UO, an LNG gas tanker discharges its product to a coastal deposit using
73 fixed loading arms with large diameters. The LNG can be re-distributed from the shore to other ships
74 through StS operations employing lower quantities and smaller loading arms. Alternatively, an LNG
75 truck can be connected to the receiving ship on the quayside (TTS). In this operation, flexible hoses are
76 used and lower LNG volumes are transferred. When a fixed structure is not present, the LNG can be
77 delivered to the receiving vessels by another ship, boat or barge (StS). Here, flexible hoses are usually
78 employed. For the dispersion of vapour, results given by deterministic procedures or over-simplified
79 models are often considered as unreliable. Indeed, the European Maritime Safety Agency (EMSA)
80 (European Maritime Safety Agency, 2017) suggests the use of detailed numerical models based on the
81 computational fluid dynamics (CFD) approach. On the other hand, consequence analyses are commonly
82 performed utilizing more user-friendly and simplified tools, namely the model Unified Dispersion
83 Model (UDM). The mentioned tools can both be used to assess the stand-off distance in terms of the
84 maximum distances at which the flammable cloud reaches the lower flammability limit (LFL) (D_{LFL}),
85 as suggested by the ISO 20519: 2017 (ISO 20519, 2017).

86 Despite the existing guidelines, several aspects involving the estimation of the safety zone are still
87 unclear or arguable. Thus, several efforts have been made to define robust procedures based on the
88 evaluation of phenomenological aspects (Jeong et al., 2020) (Jeong et al., 2018). The presence of
89 obstacles suggests the implementation of a 3D representation of the layout analyzed. Some examples

90 of the implementation of a simplified 3D layout for the evaluation of methane dispersion can be found
 91 in the current literature (Baalisampang et al., 2019) (Carboni et al., 2021b).

92 This work is devoted to the numerical characterization of the cloud dispersion and, thus, the boundaries
 93 of the safety zone resulting from the accidental release of pure methane. The assessment of the safety
 94 zones was addressed in typical bunkering and transfer operations, which were differentiated and
 95 characterized in terms of specific parameters. At this scope, different approaches were applied starting
 96 from the procedure outlined by the Society for Gas as a Marine Fuel (SGMF). In particular, a CFD
 97 software that calculates the dispersion of vapour was chosen to include the presence of obstacles in the
 98 analysis. In addition, simplified approaches were used to compare the obtained results.

99 2. Methodology

100 2.1 Source term

101 The continuous release through an orifice was assumed a reversible adiabatic expansion (i.e., isentropic
 102 expansion). Considering that it is very unlikely that the flow of a liquid could be choked, the pressure
 103 in the orifice was supposed to be atmospheric. The following equations describe the expansion to the
 104 conditions in the orifice from the initial state (i) in which the methane was supposed at saturated
 105 conditions. More specifically, Equation 1 expresses the mass releasing flowrate (\dot{m}) and Equation 2 and
 106 Equation 3, the enthalpy (H_0) and the volume (V_0) in the orifice:

$$107 \quad \dot{m} = C_d \cdot A_0 \cdot \frac{1}{V_0} \sqrt{2 \cdot (H_i - H_0)} \quad (1)$$

$$108 \quad H_0 = H(T_0, P_0, F_{L0}) \quad (2)$$

$$109 \quad V_0 = V(T_0, P_0, F_{L0}) \quad (3)$$

110 where C_d stands for the discharge coefficient, A_0 for the area of the orifice, T_0, P_0, F_{L0} for the
 111 temperature, the pressure, and the liquid fraction of the methane in the orifice, respectively. For
 112 incompressible fluids, a value of 0.6 is used for the discharge coefficient, following the literature (Uijt
 113 and Ale, 2005). The LNG leak can occur in different positions along with the systems and,
 114 consequently, have different orientations (i.e., vertical upwards/downwards, or horizontal). In the case
 115 of a vertical downward release, it is supposed that a pool is formed on a substrate, typically made by
 116 concrete or water. The formation of a vapour layer was assumed from the resulting liquid pool.
 117 Presuming the absence of mitigations systems, the pool footprint was assumed circular with radius $r(t)$,
 118 with a uniform thickness $h(t)$, related by Equation 4. In the conservation of the mass (Equation 5), the
 119 pool increases due to \dot{m} , and reduces because of pool evaporation E_{vap} (Equation 6) and dissolution on
 120 water (E_{sol}) (in case of release on water). E_{vap} is defined in Equation 6 based on power involved in
 121 boiling Q_{boil} , calculated as the net contribute of different heat transfer mechanisms (Equation 7).
 122 Conduction (Q_{cond}) from the ground was modelled assuming a uniform semi-infinite medium on which
 123 the pool spreads (Shaw and Briscoe, 1978).

$$124 \quad M_{pool}(t) = \pi \cdot r^2(t) \cdot h(t) \cdot \rho_L \quad (4)$$

$$125 \quad \frac{dM_{pool}(t)}{dt} = \dot{m}(t) - E_{vap}(t) - E_{sol}(t) \quad (5)$$

$$126 \quad E_{vap}(t) = \frac{\max(Q_{boil,0})}{\Delta H_V(T_{pool})} \quad (6)$$

$$127 \quad Q_{boil} = Q_{cond} + Q_{conv} + Q_{rad} + Q_{sol} + Q_{spill} \quad (7)$$

128 where t is the time, $M_{pool}(t)$ is the pool mass, ρ_L the density of the liquid, ΔH_V the heat of vaporization
 129 calculated as a function of the pool temperature (T_{pool}). The theory based upon Dodge et al. (1983)
 130 (Dodge et al., 1983) was used to consider the thermal contribute due to the dissolution (Q_{sol}). The
 131 method of Reid and Smith (Reid and Smith, 1978) was applied for the calculation of Q_{cond} . The method
 132 of Fleischer (1980) (Fleischer, 1980) was employed to calculate the power related to convection from
 133 the air into the pool Q_{conv} . Regarding the radiative contribute Q_{rad} , it is considered that the pool may

134 gain heat from solar radiation and longwave radiation which may also make a small contribution.
 135 Moreover, for the spill-related contribute Q_{spill} , it is considered the diverse thermal capacity between the
 136 condition at the spill and the ones in the pool. Please consider that the thermal contribute due to ice
 137 formation was neglected because of the size of the water basin, as suggested by experimental and
 138 theoretical analyses (Vesovic, 2007). For the sake of conservative results, the times maximizing the
 139 pool dimensions and the evaporation rate were considered.

140 2.2 Consequence analyses

141 Typical examples of a consequence modelling tool that employ the Unified Dispersion Model (UDM)
 142 is PHAST (Process Hazard Analysis Software Tool) by DNV-GL (DNV, 2021). The main advantages
 143 of this software stand in an extensive validation (Witlox et al., 2012) and a user-friendly interface.
 144 Nevertheless, these models cannot account for complex terrain geometries and spatial obstacles in the
 145 model domain (Gerbec et al., 2021). On the other hand, Fire Dynamics Simulator represents an open-
 146 source code for CFD analyses, validated for the characterization of the safety of cryogenic systems
 147 (McGrattan et al., 2017) (McGrattan et al., 2019b). FDS solves numerically a form of the Navier-Stokes
 148 equations appropriate for low-speed thermally-driven flow. The formulation of the equations and the
 149 numerical algorithm are contained in the FDS Technical Reference Guide (McGrattan et al., 2017). In
 150 addition, some verified and validated models are discussed in the Verification (McGrattan et al., 2013)
 151 and Validation (McGrattan et al., 2019b) guides. Besides, it can be integrated with specific sub-models
 152 devoted to accurate estimations of peculiar phenomena occurring at the investigated conditions
 153 (Carboni et al., 2021a) (Pio et al., 2019). For the LNG case, numerical estimations have been compared
 154 with large-scale experimental campaigns, i.e., Burro, Coyote, Falcon, Maplin Sands (McGrattan et al.,
 155 2019b), as reviewed by Luketa-Hanlin (Luketa-Hanlin, 2006).

156 2.3 Boundary Conditions

157 Three different scenarios involving an LNG transfer operation were investigated: 1) LNG Unloading
 158 Operation (UO); 2) LNG Shore to Ship (STS); 3) Truck to Ship (TTS) bunkering operations. In this
 159 perspective, different ships and transfer conditions were considered (Table 1). More specifically,
 160 simplified geometries based on the overall dimensions preventing the expansion of the flammable cloud
 161 were assumed as representative for the analysed ships.

162 **Table 1.** Ships involved in the present study and corresponding transfer conditions. The main characteristics
 163 should be intended as simplified overall geometrical features and with the aim of a generic example.

	Unloading Operation (UO)	Shore to Ship (STS)	Truck to Ship (TTS)
Name	JS INEOS INTREPID	-	HYPATIA DE ALEJANDRIA
IMO	9685449	-	9498755
Vessel type	LNG tanker	LNG tanker	LNG ferry
Length overall [m]	180.0	86.0	186.0*
Height overall [m]	9.0	6.0 and 11.0	17.0
Breadth overall [m]	26.6	26.7	25.0
Manifold to bow distance [m]	96.4	49.6	158
Inventory [m³]	27500	32000	40
Transfer system	Loading arm	Loading arm	Flexible hose
Transfer system diameter [inch]	12	6	2
Transfer pressure [barg]	7.55	5.55	12.00
Pool dimensions (x-direction, y-direction) [m]	4.0 x 1.6	2.0 x 1.6	2.0 x 1.6
E_{vap} [kg s⁻¹m⁻²]	0.10	0.08	0.08

164 *Length on the water line equal to 172m. The last 14m of the stern was considered 0.5m above the water.

166 Regardless of the considered operations, the ship to quayside distance and the quayside height were set
 167 equal to typical values of 1.6 m (d_{q-s}) and (h_q) 2.0 m, respectively. Moreover, for the TTS case, the
 168 truck-ship distance ($L_{f.h.}$) was posed equal to 15 m. The total volume transferred was estimated based on
 169 the analysed scenario, the type of the transfer system (i.e., flexible hoses or loading arms), the dimension
 170 of the transfer system, and the transfer pressure. The initial event was defined following the procedure
 171 suggested by the Society for Gas as a Marine Fuel (SGMF) (Bond et al., 2018), defining the worst-case
 172 scenario described in the deterministic approach of ISO 20519: 2017 (ISO 20519, 2017) as non-
 173 credible. Hence, the latter was neglected in consequence analyses performed in this work. Besides, a
 174 series of hole sizes depending on the size and the material of the loading arm (i.e., flexible or hard) is
 175 investigated. Then, the source model reported in Equation 1 was implemented to estimate the mass
 176 releasing flowrate (\dot{m}) for each scenario assuming pure methane, as commonly made in a numerical
 177 investigation (Pio and Salzano, 2018). Indeed, the presence of heavier hydrocarbons (e.g., ethane and
 178 propane) leads to smaller and less-lasting flammable clouds because of the compensation between
 179 decreased volatility and lower flammability limits (Eberwein et al., 2020). Hence, in the absence of an
 180 ignition source, pure methane can be considered as a representative of LNG.

181 Regarding the atmospheric conditions, an ambient temperature equal to 25 °C and the atmospheric
 182 Pasquill classes D (neutral), associated with a wind velocity equal to 5 m s⁻¹, and a relative humidity
 183 equal to 40% were implemented as per the case of dry and sunny conditions. On the other hand, the
 184 atmospheric Pasquill class F (very stable), associated with a wind of 2 m s⁻¹, and a relative humidity
 185 equal to 70 %, were implemented for the case of wet and foggy climatic conditions. In this view, eight
 186 scenarios for each operation (i.e., UO, STS, and TTS) were distinguished (Table 2).

187 **Table 2.** Main characteristics of the scenarios analyzed (UO, STS and TTS) in the 8 set of conditions.

Scenario	1	2	3	4	5	6	7	8
Wind [m s ⁻¹]	5	2	5	2	5	2	5	2
Pasquill	D	F	D	F	D	F	D	F
Surface	Concrete	Concrete	Concrete	Concrete	Water	Water	Concrete	Concrete
Direction	Horizontal	Horizontal	Downward	Downward	Downward	Downward	Upward	Upward

188

189 The dispersion results were expressed in terms of downwind distance to LFL (4.4% v/v) and 0.5 LFL
 190 (D_{LFL} and $D_{0.5 LFL}$) and maximum height at the LFL and 0.5 LFL (H_{LFL} and $H_{0.5 LFL}$). Furthermore, the
 191 resulting total volumes of the vapour cloud at LFL and 0.5 LFL (V_{LFL} and $V_{0.5 LFL}$) were derived. At
 192 this aim, where the loading arm is employed (i.e., UO and STS), the volumes can be calculated
 193 considering a circular base area with a diameter equal to D_{LFL} and $D_{0.5 LFL}$ respectively and a height
 194 equal to H_{LFL} and $H_{0.5 LFL}$. On the other hand, for the TTS bunkering, it is necessary to take into
 195 consideration the flexible hose length ($L_{f.h.}$) and that part of the safety zone boundaries is always
 196 defined by the scenarios involving water as substrate (Equation 8):

$$197 V_{LFL,i} = \left[\left(\frac{\pi D_{LFL,i}^2}{2} \right) + (2D_{LFL,i} \cdot L_{f.h.}) \right] \cdot H_{LFL,i} + \left(\frac{\pi D_{LFL,water}^2}{2} \right) \cdot H_{LFL,water} \text{ with } i \neq 5,6 \quad (8)$$

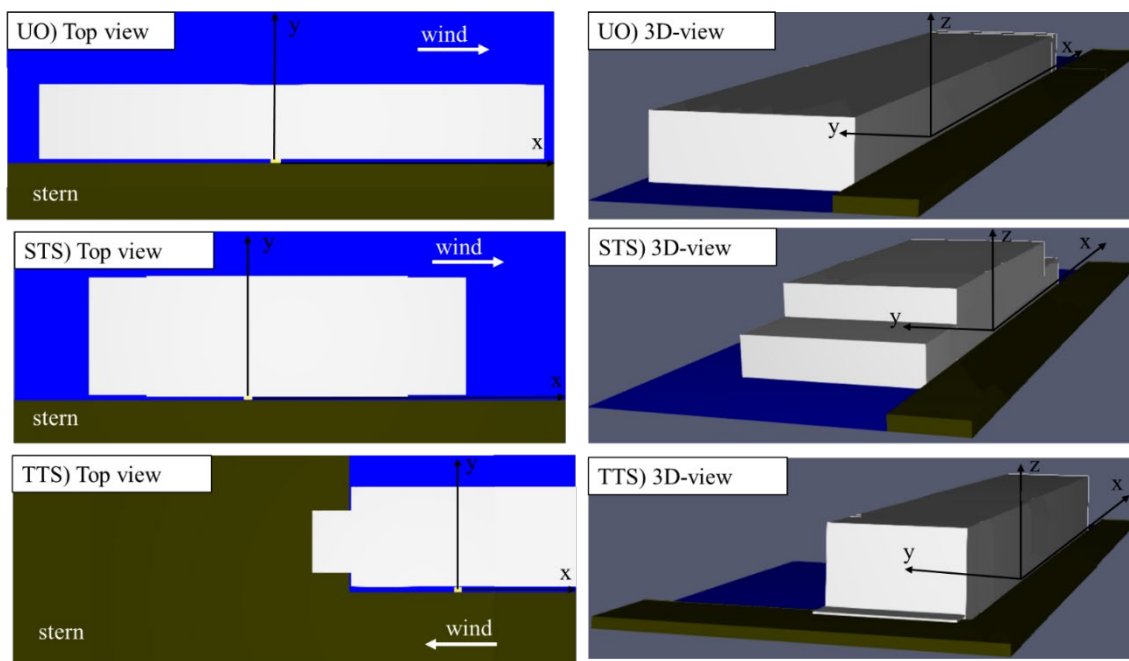
198 where $D_{LFL,water}$, and $H_{LFL,water}$ are the distances calculated for TESTs 5 and TESTs 6.

199 CFD analyses were performed posing particular attention to the release on water. This specific situation
 200 may largely affect D_{LFL} and H_{LFL} , since high evaporation rate values and significant effects of obstacles
 201 and degree of congestion are expected. Numerical results were reported at the time maximizing the
 202 stand-off distances unless otherwise noted.

203 The LNG pool was supposed to be formed between the ship and the quayside in correspondence with
 204 the ship manifold. The centre of the pool was considered as the axis origin. The size of the pool on y-
 205 direction was equalized to d_{q-s} and, the size on x-direction was derived by Equation 4. The evaporation
 206 rate was derived by Equation 5. A given value for the heat flux from the substrate was chosen following

207 data reported for the Coyote3 test (313.5 W m^{-2}) (McGrattan et al., 2019a)(McGrattan et al., 2019b). In
 208 the case of the TTS scenario, being the ship involved an LNG ferry, the bunkering was considered as
 209 simultaneous to the disembarkation/embarkation of the passengers, as provided for in the EMSA
 210 guidelines (European Maritime Safety Agency, 2017), and thus with the unloading ramp lying on the
 211 quayside. The size of the numerical grid was kept constant (i.e., with cell sizes of $0.125 \times 0.125 \times 0.125$
 212 m). Please note that, when large areas are taken into consideration, the grid cannot be fine enough to
 213 capture the mixing processes at all relevant scales. To this aim, a subgrid-scale model is employed
 214 (Smagorinsky, 1963). The large-eddy simulation (LES) equations are derived by applying a low-pass
 215 filter, parameterized by a width, to the transport equations for mass, momentum, and energy. In FDS,
 216 the filter width is equivalent to the local cell size and is a key parameter in the models accounting for
 217 the turbulent viscosity and the reaction time scale. Additional details can be found in the mathematical
 218 model reported in the Technical Reference Guide (McGrattan et al., 2017).

219 For the sake of clarity, images representing the three situations are reported (Figure 1)



220

221 **Figure 1.** Top and lateral view of the simplified layouts adopted in this work, representative of a typical port
 222 facility during LNG transfer operations.

223 Furthermore, the differences between the safety distances calculated using the LFL and the half LFL as
 224 threshold values in the case of water substrate was quantified through Equation 9.

$$225 \frac{X_{0.5LFL,j}}{X_{LFL,j}} = \left(\sum_{k=5,6} \frac{x_{0.5LFL,k,j}}{x_{LFL,k,j}} \right) \cdot \frac{1}{2} \quad (9)$$

226 where x is the generic safety parameter (i.e., D, H, and W), j the transfer operation (i.e., UO and STS),
 227 and k the k -th set of conditions involving water as substrate (i.e., 5 and 6).

228 For the sake of comparison, the same FDS simulations were conducted without considering the presence
 229 of obstacles and thus following the same geometrical approach of PHAST. In this way, it was possible
 230 to compare the three methods better and quantify the importance of considering the obstacles. At this
 231 aim, the results produced by the three different approaches (i.e., PHAST and FDS neglecting and
 232 considering the presence of obstacles) were compared introducing the following quantities:

$$233 \chi_{FDS}^{PHAST} = \frac{X_{PHAST}}{X_{FDS \text{ no obstacles}}} \quad (10)$$

234
$$x_{FDS\ obst.}^{PHAST} = \frac{X_{PHAST}}{X_{FDS\ obstacles}} \quad (11)$$

235
$$x_{FDS}^{FDS\ obst.} = \frac{X_{FDS\ obstacles}}{X_{FDS\ no\ obstacles}} \quad (12)$$

236 To estimate the area potentially involved in skin and eyes' frostbite, the wind chill temperature ($T_{w.c.}$).
 237 was calculated. Indeed, this parameter account for the perceived temperature on human skin based on
 238 the rate of heat loss from exposed skin, i.e., combining the effect of wind and cold. The National
 239 Weather Service provides a correlation starting from the measured temperature (T) and the wind
 240 velocity (V_w) (NWS, 2021) (Equation 11):

241
$$T_{w.c.} = 35.74 + 0.6215 \cdot (32 \cdot T - 32) \cdot \frac{5}{9} - 35.75 \cdot V_w^{0.16} + 0.4275 \cdot (32 \cdot T - 32) \cdot \frac{5}{9} \cdot V_w^{0.16} \quad (10)$$

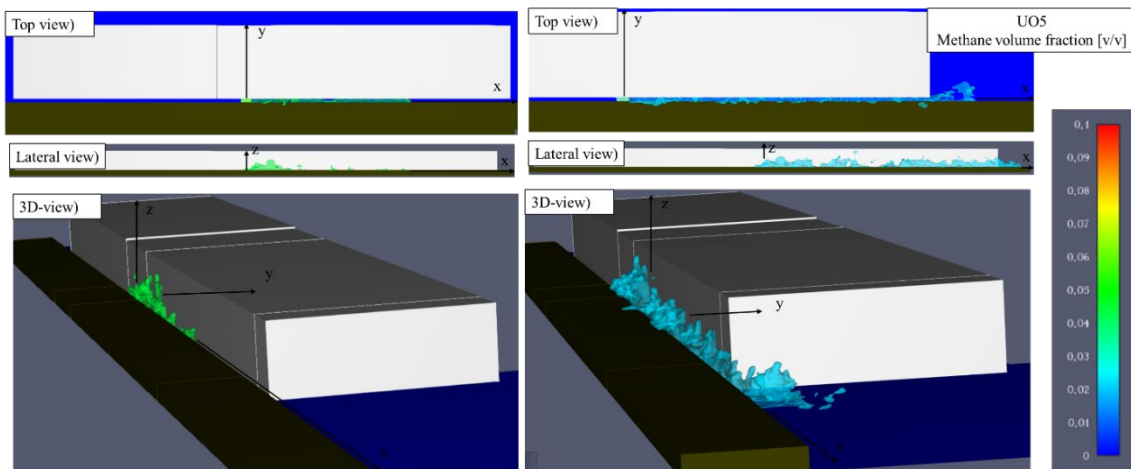
242 $T_{w.c.}$ was used to define the boundaries of an area where human-being can suffer from frostbite. More
 243 specifically the wind chill chart commonly adopted in the literature (Morris, 2007)(Kiss, 2012) was
 244 employed under the assumption of an exposure time of 5, 10, and 30 minutes.

245

246 Results and discussion

247 FDS results considering the presence of obstacles are presented at first. More specifically, results are
 248 introduced in the form of images in the following figures considering different views (i.e., top, lateral,
 249 and 3D). Then, they are presented and compared in terms of safety distances.

250 The unloading operation considering the water as substrate and 5D as atmospheric conditions (i.e., UO)
 251 is considered the base case. Figure 2 reports the methane distribution for the UO5 scenario, whereas
 252 results related to the other cases are reported in the supplementary material.



253

254 **Figure 2.** FDS results expressed in terms of methane volume fraction isosurfaces [v/v] viewed from different
 255 points in the UO5 scenario. The light blue colour cloud is the isosurface at 0.5LFL, while the green one is at LFL.

256 If the flammable cloud is limited to the area where a molar fraction higher than LFL can be found in
 257 the UO5 scenario, it is completely included within the area delimited by ship and quayside. On the other
 258 hand, the widespread assumption suggesting the use of half LFL as a threshold value to delimit the
 259 flammable area leads to a stand-off distance exceeding the ship end by 19 m on the downwind direction
 260 (positive x-direction) and 4.4 m in the perpendicular one (positive y-direction). In the 2F conditions
 261 (i.e., scenario UO6, Figure S1), a similar trend can be identified. The main difference between the two
 262 atmospheric conditions can be retrieved in the time history of flammable cloud areas. Indeed, initially,
 263 the cloud is colder, consequently heavier than air, and therefore less influenced by the wind. For this
 264 reason, the cloud spreads on both sides of the pool. In the second phase, i.e., when the temperature rises,
 265 the cloud becomes lighter than air favouring the dispersion in the downwind direction. The heat

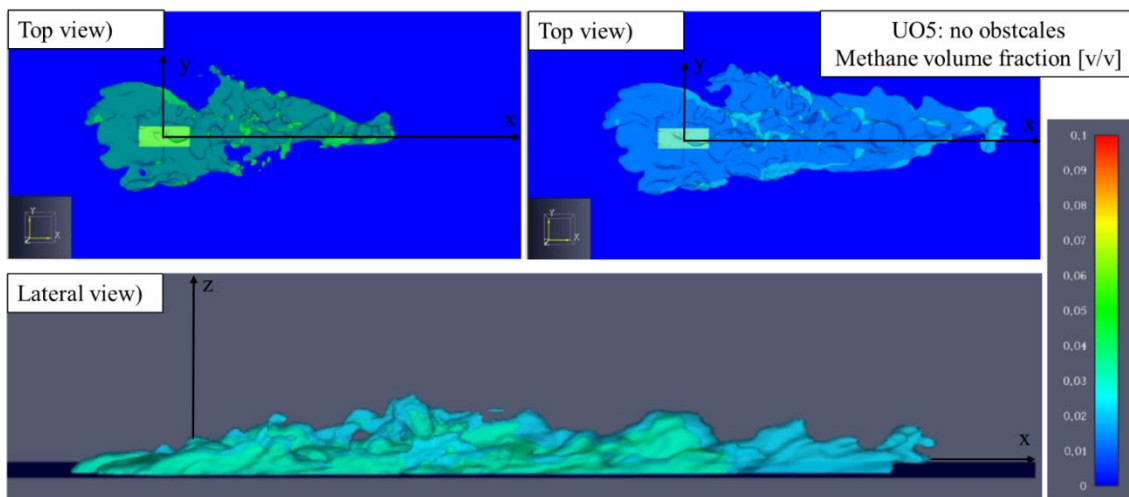
266 exchange is more effective when the wind velocity is higher, thus the spreading phase is less lasting
 267 when a 5 m s⁻¹ condition is considered. A dedicated analysis investigating these aspects will follow in
 268 this study. In both scenarios, the cloud develops its height preferentially along with the ship's walls
 269 rather than the quayside. Regarding the negative y-direction, the flammable cloud succeeds in
 270 overcoming the quayside. More specifically, it expands for 1.0 m and 3.3 m in the UO5 and UO6
 271 scenarios, respectively. In both STS5 and STS6, the flammable cloud does not exceed the overall ship
 272 dimensions (Figure S2 and Figure S3). Regarding the quayside, it is overcome by the cloud only at t₂.
 273 More specifically, it expands for 2.7 m and 2.4 m in the STS5 and STS6 scenarios, respectively.

274 Bearing in mind the shape of the resulting flammable clouds when FDS is applied considering the 3-D
 275 layout, the equation necessary to calculate the safety volume is:

$$276 \quad V_{LFL,i} = 2 \cdot [(D_{LFL,i} \cdot W_{LFL,i} \cdot H_{LFL,i}) - V_q] \quad (11)$$

277 where $W_{LFL,i}$ is the maximum width of the flammable cloud in the y-direction and V_q is the solid volume
 278 of the quayside that has to be subtracted. Factor 2 is introduced to take into consideration opposite wind
 279 directions. For the sake of the volume calculation, the maximum distances retrieved in each case were
 280 taken into consideration for the sake of conservative results.

281 The flammable clouds generated for the UO5 scenario are also evaluated in the absence of obstacles
 282 (Figure 3). The case with 2F conditions can be found in the supplementary material (Figure S4).

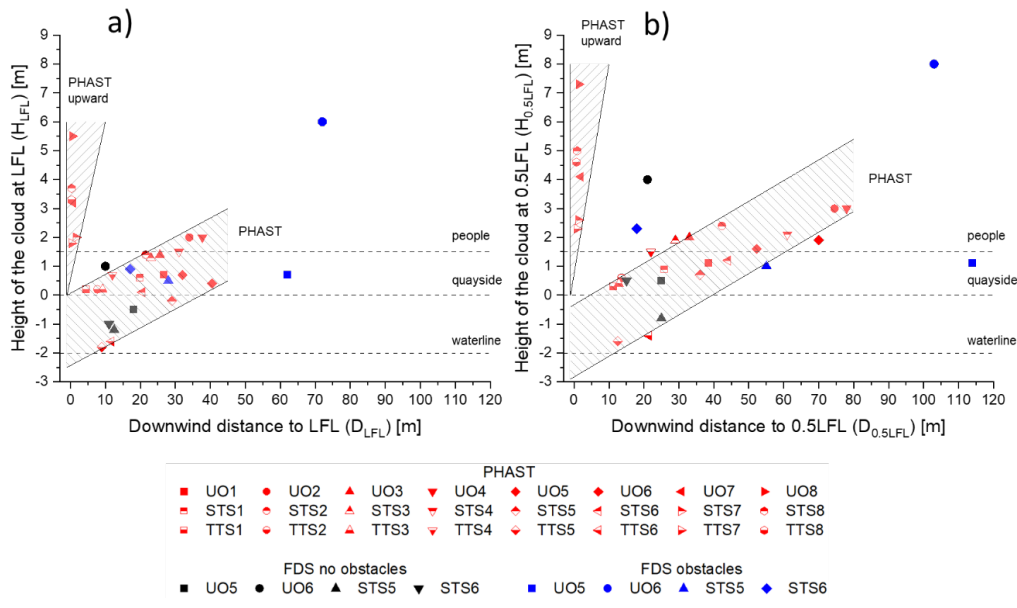


283
 284 **Figure 3.** FDS results viewed from different points in the UO5 scenario when the presence of obstacles is
 285 neglected. The light blue colour cloud is the isosurface at 0.5LFL, while the green one is at LFL.

286 When the open field is considered, the resulting flammable cloud has similar dimensions in the x and y
 287 directions. After a preliminary phase in which the cloud develops in the wind direction, stabilization is
 288 reached. Lower values of downwind distance and flammable height are obtained concerning the case
 289 with obstacles due to the lack of confinement and the ship's wall effect. Similar results are obtained for
 290 the other scenarios. Starting from these considerations, safety distances are analyzed in the following
 291 Figure 4 in terms of downwind distance and height of the flammable cloud at LFL and 0.5 LFL.
 292 Furthermore, PHAST results are added, showing two distinguishable areas based on the threshold value
 293 considered (i.e., at LFL and 0.5 LFL). The first is characterized by a high and concentrated cloud,
 294 whereas the second shows a wider area. The scenarios that produce maximum D_{LFL} and H_{LFL} are the
 295 UO5 (40.5 m) and UO8 (5.5 m), respectively, identifying the UO as the operation that involves the
 296 largest safety area. On the other hand, the safety distances calculated in terms of the 0.5 LFL show a
 297 maximum $D_{0,5LFL}$ for UO4 and UO6 (i.e., 78 m and 70 m, respectively). These results confirm the on-
 298 water release as the one requiring particular attention. Conversely, the TTSs are intrinsically safer.

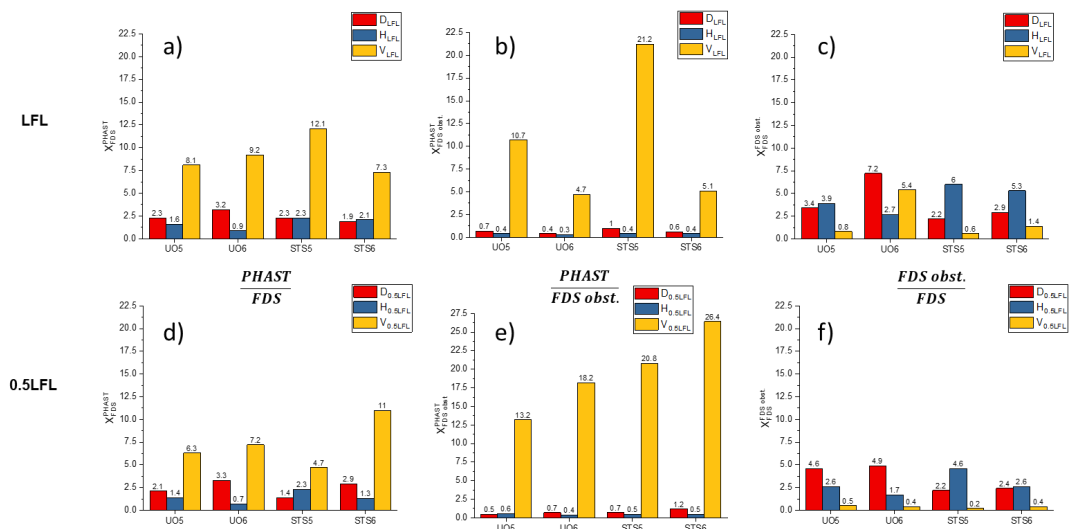
299 Regarding results obtained utilizing FDS, only the cases where obstacles are included provide larger
 300 areas than the ones obtained by PHAST at any corresponding conditions. Conversely, in the absence of
 301 obstacles (as it is for PHAST), FDS produces significantly narrower safety zones are obtained.

302 The UO scenarios produce larger areas with all the approaches considered, followed by STS. Regarding
 303 PHAST, TESTs 7 and 8 (vertical release) yield low values of safety volume except for the TTS scenario
 304 due to the different systems employed and thus different ways of the volume calculation. Additional
 305 details on the resulting safety volumes can be found in Figure S5. When the CFD is applied, safety
 306 volumes are dramatically reduced, and the lowest values are obtained when the obstacles are considered.
 307 Furthermore, 2F atmospheric conditions are not the most conservative in all the investigated scenarios.



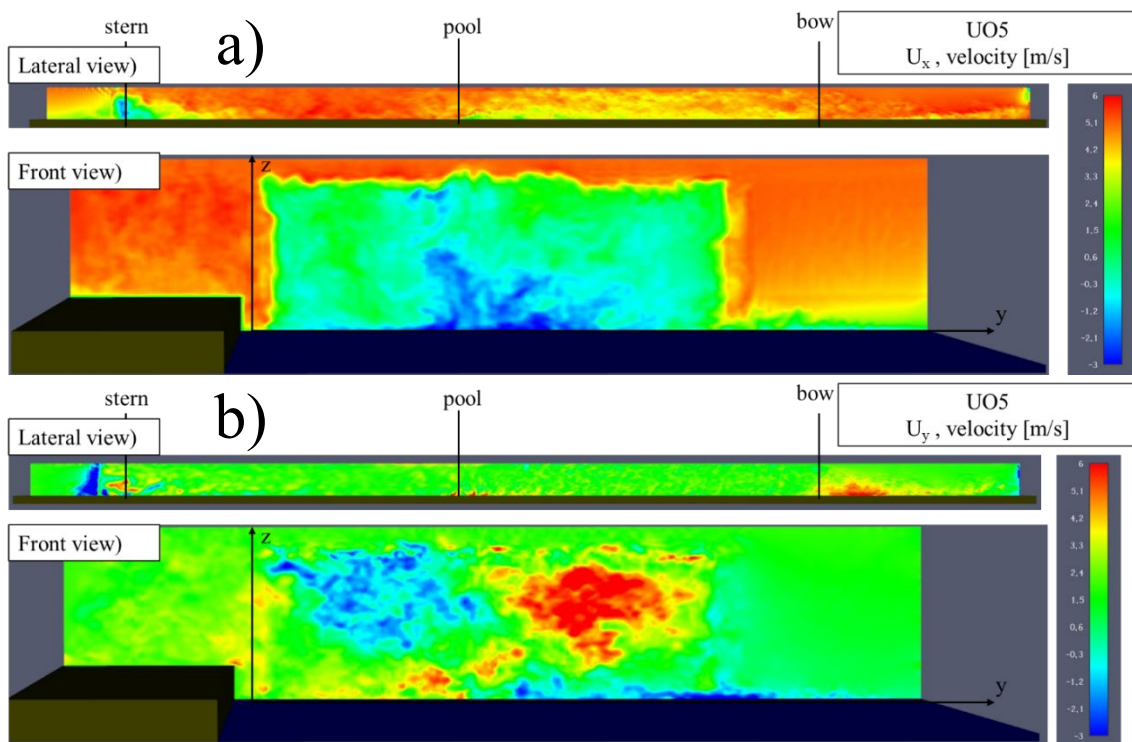
308 **Figure 4.** PHAST, FDS, and FDS with obstacles results expressed in terms of downwind distance and height of
 309 the flammable cloud at LFL (a) and 0.5 LFL (b).
 310

311 The safety distances obtained by different methods are compared in Figure 5.



312 **Figure 5.** Safety distances at LFL (first row) and 0.5LFL (second row) produced by the three different approaches
 313 (i.e., PHAST and FDS neglecting and considering the presence of obstacles) applied to the scenarios considering
 314 water as substrate (i.e., 5 and 6).
 315

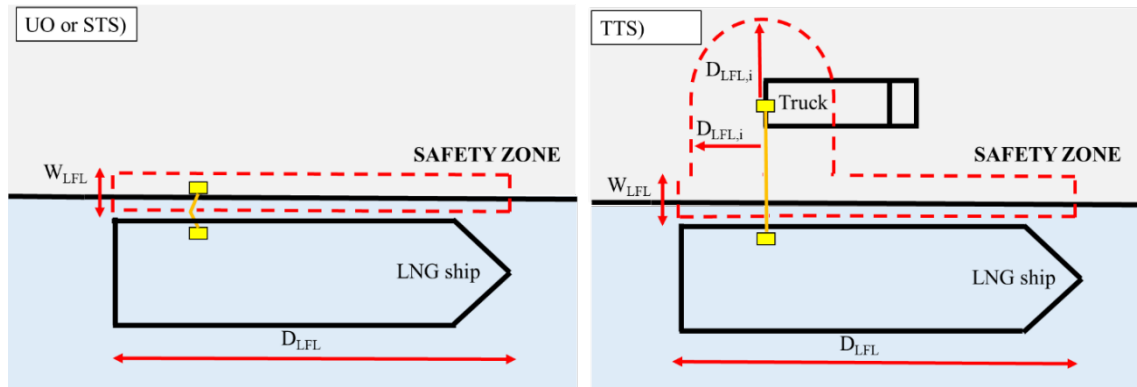
316 PHAST produces almost double H and D than the case without obstacles evaluated by FDS. On the
 317 other hand, when the obstacles are introduced, estimated distances turn out to be higher than PHAST.
 318 Nevertheless, it is worth noting that PHAST provides larger volumes for any scenarios, meaning that
 319 larger areas reported once obstacles are considered in FDS simulations are mainly due to the congestion.
 320 A similar conclusion can be drawn when the two FDS approaches are compared. Consequently, the
 321 main positive aspect of the adoption of CFD models considering a real layout is the identification of the
 322 specific portion of volume involved in the cloud expansion. Indeed, depending on the wind direction,
 323 the presence of obstacles can narrow the flammable area in any direction perpendicular to the ship.
 324 In the proximity of the quayside, the safety zone should be extended for all the overall length of the ship,
 325 since in all the simulations, this zone is characterized by methane mole fractions larger than 0.5 LFL.
 326 On the other hand, these values are not reached beyond the ship, and thus the safety zone boundary in
 327 the y -direction can be identified by the ship wall. The presence of ship walls affects the velocity
 328 distribution, as reported in Figure 6 for the UO5 case at the time maximizing the downwind distances.



329 **Figure 6.** Velocity in the x -direction (U_x) (a) and the y -direction (U_y) (b) of the UO5 scenario displayed from
 330 lateral and front. Please note that the Front view reports data obtained at 5 m from the bow in the downwind
 331 direction.
 332

333 Observing the lateral view, the regions where smaller rates can be found correspond to the fuel-rich
 334 pockets. This trend is attributable to fluid dynamics aspects since cold methane is denser than air in the
 335 proximity of the releasing point. On the other hand, the decreasing content of methane in the mixture,
 336 together with its increasing temperature, reduces this effect at a far-field distance. The combination of
 337 the U_x and U_y reported in Front views indicates the intensity of mixing phenomena induced by the
 338 expansion of the area available to the vapour. Indeed, Figure 7 confirms the presence of recirculating
 339 section since largely negative values can be observed for U_x , meaning that in a portion of the
 340 investigated section methane travels in the upwind direction. Similarly, Figure 8 shows largely positive
 341 U_y (up to 6 m s^{-1}) from the down-left corner to the top-right corner, whereas largely negative U_y (up to
 342 -6 m s^{-1}) in the direction symmetric to the z -axis, although in this case, the component of the wind
 343 speed on the y -axis is null. Besides, the latter phenomena may extend the safety distances on the y -
 344 direction (W_{LFL}). This parameter should be defined taking into consideration the specific case since it
 345 is strictly dependent on h_q . In the case of a flexible hose as a transfer system, an on-land release is not
 346 negligible. Starting from these considerations, the safety zone should be extended accordingly, taking

347 into consideration the release direction that produces more considerable distances (k-th set of conditions
 348 with $k \neq 5,6$). A simplified schematization is presented in Figure 7.



349
 350 **Figure 7.** Safety zone application in case of use of a loading arm (left, UO, and STS) or flexible hose (right, TTS).

351 These results are conservative on the safe side if different wind directions and velocities are considered.
 352 Indeed, when the wind blows from the north-west or southwest at 5 m s^{-1} lower values of downwind
 353 distances are obtained (Figure S7). On the other hand, when the high wind velocity is considered (i.e.,
 354 10 m s^{-1}) similar downwind distances and lower height are obtained (Figure S8). According to the
 355 international standards (ISO 20519, 2017), the safety zone is assumed as a circular shape with a radius
 356 equal to D_{LFL} , when a loading arm is employed. Similarly, an elliptical-like shape is considered when a
 357 flexible hose is employed, having a semicircular extremity of D_{LFL} and centre-to-centre distance $L_{f,h}$. A
 358 visual representation of these cases is reported in supplementary materials (Figure S6).

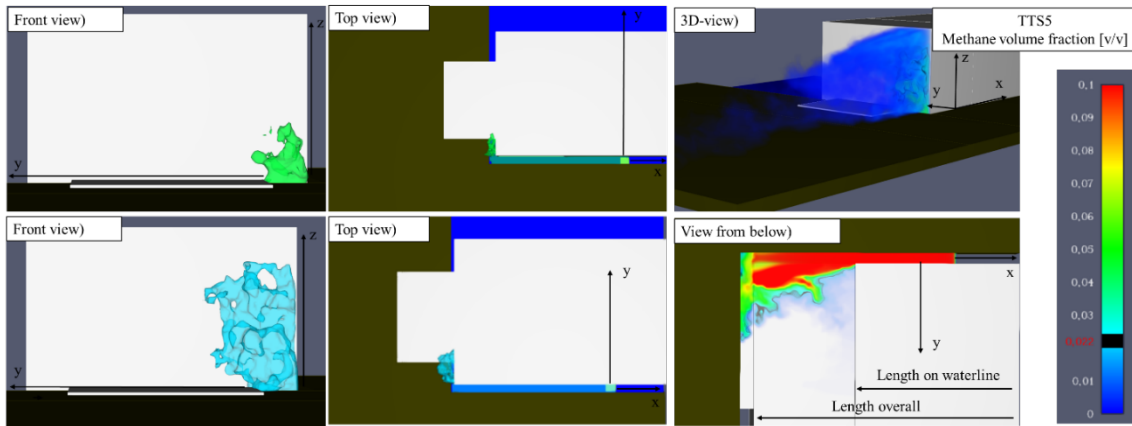
359 Regarding the differences in considering the beginning of the flammability concentration (i.e., 0.5 LFL)
 360 instead of lethality (i.e., LFL), it is possible to averagely consider the values reported in Table 7
 361 expressed in terms of $\frac{D_{0.5 LFL}}{D_{LFL}}$, $\frac{H_{0.5 LFL}}{H_{LFL}}$ and $\frac{W_{0.5 LFL}}{W_{LFL}}$.

362 **Table 3.** FDS results expressed in terms of $\frac{D_{0.5 LFL}}{D_{LFL}}$, $\frac{H_{0.5 LFL}}{H_{LFL}}$ and $\frac{W_{0.5 LFL}}{W_{LFL}}$.

TEST	$\frac{D_{0.5 LFL}}{D_{LFL}}$			$\frac{H_{0.5 LFL}}{H_{LFL}}$			$\frac{W_{0.5 LFL}}{W_{LFL}}$		
	PHAST	FDS	FDS Obst.	PHAST	FDS	FDS Obst.	PHAST	FDS	FDS Obst.
UO	1.7	1.7	1.6	1.5	1.8	1.2	2.2	1.0	1.6
STS	1.7	1.7	1.4	1.5	2.0	1.3	2.1	1.0	1.2

363
 364 Quite similar ratios are obtained when the downwind distances are evaluated regardless of the method
 365 considered. On the other hand, when the heights of flammable clouds are examined large differences
 366 can be detected between the two CFD approaches. On y-direction (W), FDS (neglecting obstacles)
 367 produces similar clouds when the two thresholds are analyzed, whereas PHAST produces more than
 368 double areas. The introduction of obstacles in FDS results in an intermediate condition between the two
 369 alternative approaches discussed before.

370 As already reported in this work, one of the typical circumstances that are worth to be analysed is the
 371 disembarkation of an LNG ferry during a bunkering procedure. In this configuration, the quayside is
 372 also present in the proximity of the stern, where the disembarkation ramp is placed. In Figure 8, the
 373 flammable region in this configuration is presented for the 5D atmospheric class, whereas the case with
 374 2F can be found in the supplementary material (Figure S9).



375

376 **Figure 8.** Methane distribution as obtained by FDS for the TTS5 scenario. Please note that the light blue colour
 377 cloud is the isosurface at 0.5 LFL, whereas the green one is at LFL.

378 As it is possible to note from Figure 10, the flammable cloud reaches the disembarkation ramp since
 379 the manifold is in proximity to the stern. Hence, part of the flammable cloud reaches passengers. Quite
 380 clearly, it is possible to affirm that this area is the most critical for the co-existence of an elevated grade
 381 of congestions and the possible presence of passengers and vehicles. The latter can also be intended as
 382 an additional source of ignition. For these reasons, specific barriers or mitigation systems (e.g., water
 383 curtain) should be considered. Based on the typical geometry of the investigated ship, a height of 0.5 m
 384 on the water level was implemented (view from below of Figure 10). This permits us to consider the
 385 expansion of the cloud in this area and observe that a high methane concentration in the air is methane
 386 (i.e., larger than 0.1 v/v). Furthermore, flammable areas are observed above the ramp (front view of the
 387 ship), contributing to increasing the concerns on this area. However, no significant expansion on the
 388 quayside is observed.

389 Considering the presented results, only the temperature distribution obtained for the TTS5 scenario is
 390 reported in this manuscript. Indeed, the TTS5 scenario represents the only case where a detailed analysis
 391 on possible frostbite is necessary, because of the coexistence of passengers without specific protective
 392 clothing and cold vapours in the proximity of the quayside. At this aim, the frostbite danger was assessed
 393 at different wind velocities (V_w) and exposure times. The resulting safety distances from the pool centre
 394 were reported in Table 4.

395 **Table 4.** Frostbite safety distances (m) as a function of wind velocity (ms^{-1}) and exposure time (min).

Wind velocity (V_w) [m s^{-1}]	Frostbite safety distances [m]		
	5 min	10 min	30 min
5	11	16	22
10	13	18	22
15	15	19	23
20	17	19	23
25	18	21	24

396

397 Based on the reported results it is possible to conclude that frostbite does not represent a significant
 398 issue from a safety perspective for LNG bunkering procedures, even in the case of simultaneous
 399 disembarking. Indeed, the related distances are included in the flame envelope considered for the
 400 assessment of safety distances for the flash fire scenario also in the case of large exposure time.

401 Conclusions

402 This article presents a numerical characterization of the safety aspects related to an accidental release
 403 of liquefied natural gas in port areas under a wide range of conditions, in absence of an ignition source.
 404 In particular, different layouts representative for ships, as well as alternative operations, potentially used

405 for cryogenic fuels were analysed through the implementation of three-dimensional structures in
406 computational fluid dynamics, integrated by sub-models suitable for cryogenic conditions. The obtained
407 fuel distribution was used for the evaluation of the safety distance related to a flash fire, whereas the
408 combination of temperature distribution and wind speed was used to individuate the area potentially
409 involved by frostbite. Results deriving from integral and discrete approaches were compared in terms
410 of safety distances, flammable volume, and size under the hypothesis commonly adopted for the
411 characterization of flash fire. Although the introduction of obstacles leads to an increase in the
412 flammable region, all of them were found to be limited to the proximity of the ships. This phenomenon
413 was attributed to the increased effectiveness in fuel-air mixing, as testified by the velocity distribution
414 reported in this work. Eventually, the possible presence of passengers within the flammable area
415 deriving from an accidental release under the investigated conditions was detected only for the Truck
416 to Ship bunkering operations, suggesting the installation of proper mitigation systems. Hence, the
417 current study provides a robust and phenomenological-based background for the realization of safe
418 infrastructures and procedures dealing with cryogenic fuels.

419 **References**

- 420 Aneziris, O., Koromila, I., Nivolianitou, Z., 2020. A systematic literature review on LNG safety at ports. *Saf.*
421 *Sci.* 124, 104595. <https://doi.org/10.1016/j.ssci.2019.104595>
- 422 Baalisampang, T., Abbassi, R., Garaniya, V., Khan, F., Dadashzadeh, M., 2019. Accidental release of Liquefied
423 Natural Gas in a processing facility: Effect of equipment congestion level on dispersion behaviour of the
424 flammable vapour. *J. Loss Prev. Process Ind.* 61, 237–248. <https://doi.org/10.1016/j.jlp.2019.07.001>
- 425 Bond, S., Boon, C., Boreman, J., Dalkakis, D., de Souza, C., Eiermann, G., Eltringham, J., Haynes, D.,
426 Jaerschel, D., Johnson, M., LaRoche, M., Linsner, E., Peeters, R., Garrido, G.L., 2018. Gas as a marine
427 fuel - Recommendation of Controlled Zones during LNG bunkering, *Energy Policy*.
428 <https://doi.org/10.1016/j.enpol.2015.08.027>
- 429 Carboni, M., Pio, G., Mocellin, P., Vianello, C., Maschio, G., Salzano, E., 2021a. On the flash fire of stratified
430 cloud of liquefied natural gas. *J. Loss Prev. Process Ind.* 75, 104680.
431 <https://doi.org/10.1016/j.jlp.2021.104680>
- 432 Carboni, M., Pio, G., Vianello, C., Salzano, E., 2021b. Safety distances for the sour biogas in digestion plants.
433 *Process Saf. Environ. Prot.* 147, 1–7. <https://doi.org/10.1016/j.psep.2020.09.025>
- 434 Chang, Y.T., Park, H., 2019. The impact of vessel speed reduction on port accidents. *Accid. Anal. Prev.* 123,
435 422–432. <https://doi.org/10.1016/j.aap.2016.03.003>
- 436 Chen, Z., Zhang, F., Xu, B., Zhang, Q., Liu, J., 2017. Influence of methane content on a LNG heavy-duty engine
437 with high compression ratio. *Energy* 128, 329–336. <https://doi.org/10.1016/j.energy.2017.04.039>
- 438 DNV, 2021. Process Hazard Analysis Software Tool (PHAST) [WWW Document]. URL
439 <https://www.dnv.com/software/services/phast/index.html> (accessed 5.1.21).
- 440 Dodge, F.T., Park, J.T., Buckingham, J.C., Maggott, R.J., 1983. Revision and experimental verification of the
441 hazard assessment computer system models for spreading, movement, dissolution and dissipation of
442 insoluble chemicals spilled onto water, US Coast Guard Report CG-D-35-83.
- 443 Eberwein, R., Rogge, A., Behrendt, F., Knaust, C., 2020. Dispersion modeling of LNG-Vapor on land – A CFD-
444 Model evaluation study. *J. Loss Prev. Process Ind.* 65, 104116.
445 <https://doi.org/https://doi.org/10.1016/j.jlp.2020.104116>
- 446 European Maritime Safety Agency, 2017. Guidance on LNG Bunkering to Port Authorities and Administration.
447 31 January 430.
- 448 Fleischer, F.T., 1980. SPILLS: An evaporation/air dispersion model for chemical spills on land, Shell
449 Westhollow Research Center, Houston, Texas.
- 450 Fy, G., Wand, J., Yan, M., 2016. Anatomy of Tianjin Port Fire and Epllosion: Process and Caused. *Process Saf.*
451 *Prog.* 35. <https://doi.org/10.1002/prs>
- 452 Gerbec, M., Vidmar, P., Pio, G., Salzano, E., 2021. A comparison of dispersion models for the LNG dispersion
453 at port of Koper, Slovenia. *Saf. Sci.* 144, 105467. <https://doi.org/10.1016/j.ssci.2021.105467>
- 454 ISO 20519, 2017. ISO 20519 Ships and marine technology — Specification for bunkering of liquefied natural
455 gas fuelled vessels Navires 2017.
- 456 Jeong, B., Lee, B.S., Zhou, P., Ha, S. man, 2018. Determination of safety exclusion zone for LNG bunkering at
457 fuel-supplying point. *Ocean Eng.* 152, 113–129. <https://doi.org/10.1016/j.oceaneng.2018.01.066>
- 458 Jeong, B., Park, S., Ha, S., Lee, J. ung, 2020. Safety evaluation on LNG bunkering: To enhance practical
459 establishment of safety zone. *Ocean Eng.* 216, 107804. <https://doi.org/10.1016/j.oceaneng.2020.107804>
- 460 Kiss, T.L., 2012. Critical Care for Frostbite. *Crit. Care Nurs. Clin. North Am.* 24, 581–591.

461 <https://doi.org/https://doi.org/10.1016/j.ccell.2012.07.001>
462 Kumar, P., Chirayil, P.T., 1999. Helium vapour injury: A case report. *Burns* 25, 265–268.
463 [https://doi.org/10.1016/S0305-4179\(98\)00163-6](https://doi.org/10.1016/S0305-4179(98)00163-6)
464 Luketa-Hanlin, A., 2006. A review of large-scale LNG spills: Experiments and modeling. *J. Hazard. Mater.*
465 <https://doi.org/10.1016/j.jhazmat.2005.10.008>
466 McGrattan, K., Hostikka, S., McDermott, R., Floyd, J., Vanella, M., 2019a. Fire Dynamics Simulator User’s
467 Guide. NIST Spec. Publ. 1019 Sixth Ed. 347. <https://doi.org/10.6028>
468 McGrattan, K., Hostikka, S., McDermott, R., Floyd, J., Weinschenk, C., Overhold, K., 2019b. Fire dynamics
469 simulator (FDS) validation technical reference guide volume 3 : Validation. NIST Spec. Publ. 1018 3.
470 <https://doi.org/10.6028/NIST.SP.1018-1>
471 McGrattan, K., Hostikka, S., McDermott, R., Floyd, J., Weinschenk, C., Overhold, K., 2013. Fire Dynamics
472 Simulator, Technical Reference Guide, Volume 2: Verification.
473 McGrattan, K., Hostikka, S., McDermott, R., Floyd, J., Weinschenk, C., Overholt, K., 2017. Fire Dynamics
474 Simulator Technical Reference Guide Volume 1: Mathematical Model. NIST Spec. Publ. 1018-1 1.
475 <https://doi.org/10.6028/NIST.SP.1018>
476 Morris, S.E., 2007. Cold-induced injury: frostbite, in: Herndon, D.N.B.T.-T.B.C. (Third E. (Ed.)), *Cold-Induced*
477 *Injury: Frostbite*. W.B. Saunders, Edinburgh, pp. 530–535. [https://doi.org/https://doi.org/10.1016/B978-1-](https://doi.org/https://doi.org/10.1016/B978-1-4160-3274-8.50044-1)
478 [4160-3274-8.50044-1](https://doi.org/10.1016/B978-1-4160-3274-8.50044-1)
479 NWS, 2021. National Weather Service: The New Improved Wind Chill Index [WWW Document]. URL
480 <https://www.weather.gov/ffc/wci> (accessed 7.1.21).
481 Osorio-Tejada, J.L., Llera-Sastresa, E., Scarpellini, S., 2017. Liquefied natural gas: Could it be a reliable option
482 for road freight transport in the EU? *Renew. Sustain. Energy Rev.* 71, 785–795.
483 <https://doi.org/10.1016/j.rser.2016.12.104>
484 Paik, J.K., 2020. *Advanced Structural Safety Studies With Extreme Conditions and Accidents*. Springer,
485 Singapore.
486 Park, S., Jeong, B., Yoon, J.Y., Paik, J.K., 2018. A study on factors affecting the safety zone in ship-to-ship
487 LNG bunkering. *Ships Offshore Struct.* 13, 312–321.
488 <https://doi.org/https://doi.org/10.1080/17445302.2018.1461055>
489 Park, S.I., Kim, S.K., Paik FReNg, J.K., 2020. Safety-zone layout design for a floating LNG-Fueled power plant
490 in bunkering process. *Ocean Eng.* 196, 106774. <https://doi.org/10.1016/j.oceaneng.2019.106774>
491 Pio, G., Carboni, M., Iannaccone, T., Cozzani, V., Salzano, E., 2019. Numerical simulation of small-scale pool
492 fires of LNG. *J. Loss Prev. Process Ind.* 61, 82–88. <https://doi.org/10.1016/j.jlp.2019.06.002>
493 Pio, G., Salzano, E., 2019. The effect of ultra-low temperature on the flammability limits of a
494 methane/air/diluent mixtures. *J. Hazard. Mater.* 362, 224–229.
495 <https://doi.org/10.1016/j.jhazmat.2018.09.018>
496 Pio, G., Salzano, E., 2018. Laminar Burning Velocity of Methane, Hydrogen, and Their Mixtures at Extremely
497 Low-Temperature Conditions. *Energy & Fuels* 32, 8830–8836.
498 <https://doi.org/10.1021/acs.energyfuels.8b01796>
499 Publication, B.S.I.S., 2015. ISO / TS 18683 : 2015 Standards Publication Guidelines for systems and
500 installations for supply of LNG as fuel to ships.
501 Reid, R.C., Smith, K.A., 1978. Confined boiling rates of liquefied petroleum gas on water, EE-77-S-02-4548
502 MIT.
503 Sever, C., Ulkur, E., Uygur, F., Celikoz, B., 2008. Hand burn caused by Freon gas. *Burns* 34, 1210–1212.
504 <https://doi.org/10.1016/j.burns.2007.09.017>
505 Shaw, P., Briscoe, F., 1978. Evaporation from spills of hazardous liquids on land and water, SRD report R100.
506 Smagorinsky, J., 1963. General Circulation Experiments with the Primitive Equations. The Basic Experiment.
507 *Mon. Weather Rev.* 91. <https://doi.org/10.1126/science.26.653.25>
508 Uijt, H.P.A.M., Ale, B.J.M., 2005. Guideline for quantitative risk assessment ‘Purple book’.
509 Uygur, F., Sever, C., Noyan, N., 2009. Frostbite burns caused by liquid oxygen. *J. Burn Care Res.* 30, 358–361.
510 <https://doi.org/10.1097/BCR.0b013e318198a769>
511 Vesovic, V., 2007. The influence of ice formation on vaporization of LNG on water surfaces. *J. Hazard. Mater.*
512 140, 518–526. <https://doi.org/10.1016/j.jhazmat.2006.10.039>
513 Weinzweig, J., 2010. *Plastic Surgery Secrets Plus*, 2nd ed.
514 Witlox, H.W.M., Harper, M., Pitblado, R., 2012. Validation of phast dispersion model as required for USA
515 LNG siting applications. 12th Top. Conf. Gas Util. 2012 - Top. Conf. 2012 AIChE Spring Meet. 8th Glob.
516 *Congr. Process Saf.* 31, 263–275.
517